Shortcut Experimental Method for Designing Chiral SMB Separations

Cristiano Migliorini and Marco Mazzotti
ETH Zürich, Institut für Verfahrenstechnik, Sonneggstrasse 3, CH-8092 Zürich, Switzerland

Gianmarco Zenoni and Massimo Morbidelli
ETH Zürich, Laboratorium für Technische Chemie, Universitätstrasse 6, CH-8092 Zürich, Switzerland

The simulated moving-bed (SMB) chromatographic separation of the Tröger's base enantiomers with ethanol as eluent on microcrystalline triacetate cellulose was studied. An experimental technique to design nonlinear SMB separations with few column experiments is presented. This shortcut technique allows the rigorous solution of the Equilibrium Theory model to be approximated without knowing the adsorption equilibria, and therefore can be useful in developing new separations. The predictions of the shortcut method are compared with the experimental results of the SMB separation. The effect of the feed concentration and of the nonideal contributions, such as mass-transfer resistance and extracolumn band broadening, are elucidated.

Introduction

The scale-up of enantiomer separations from the batch to the continuous simulated moving-bed (SMB) process is often an important step in the development and production of a new product in the fine chemical and pharmaceutical industry. In recent years, the SMB technology has shown many advantages over batch preparative chromatography and has attracted the interest of the fine chemical industry (Negawa and Shoji, 1992; Cavoy et al., 1997; Francotte and Richert, 1997; Guest, 1997; Nagamatsu et al., 1999).

In the SMB unit, the countercurrent contact between the solid and mobile phases is achieved by periodically shifting the inlet (feed, desorbent) and outlet (raffinate, extract) ports in the direction of the fluid flow. Under complete separation conditions, the more and less retained enantiomers are collected continuously in the extract and in the raffinate, respectively (see Figure 1. The regeneration of the stationary and fluid phases in sections 1 and 4, respectively, allows them to be recycled, and therefore make a continuous operation. The advantages of the countercurrent contact between the stationary and mobile phases are a higher productivity, a lower desorbent requirement (Ruthven and Ching, 1989; Mazzotti et al., 1997), and an increased separation performance, which allows product recovery at high purities even when the selectivity is close to one or the efficiency of the stationary phase is low (Yun et al., 1997c; Pedeferri et al., 1999).

Although these properties are attractive, the key to the success of this unit operation rests on its flexibility and fast scale-up. The same SMB unit (equipped with the same or different columns) in fact can be used for many separations, allowing the parallel screening of many potential drug candidates. Moreover, under linear conditions the scale-up of the separation from the HPLC to the SMB is rather straightforward (Yun et al., 1997c; Pedeferri et al., 1999). This allows the time to develop a new product to be significantly shortened.

On the other hand, the scale-up of separations under nonlinear conditions is more difficult and may require a lengthy trial-and-error procedure (Francotte et al., 1998; Pröll and Küsters, 1998; Nagamatsu et al., 1999). However, higher productivity and a lower desorbent requirement per unit mass of product motivate this pursuit. A reliable design of the nonlinear separation based on detailed (Charton and Nicoud, 1995; Pais et al., 1997; Wu et al., 1998; Migliorini et al., 1999a) or ideal models (Francotte et al., 1998; Pedeferri et al., 1999) is possible, but it requires knowledge of the adsorption equilibria. The determination of such equilibria is time-consuming, and in addition it depends on the availability of large amounts of pure substances, and therefore it may not be feasible in the early development of a new product, particularly in the pharmaceutical industry.

Correspondence concerning this article should be addressed to M. Morbidelli.

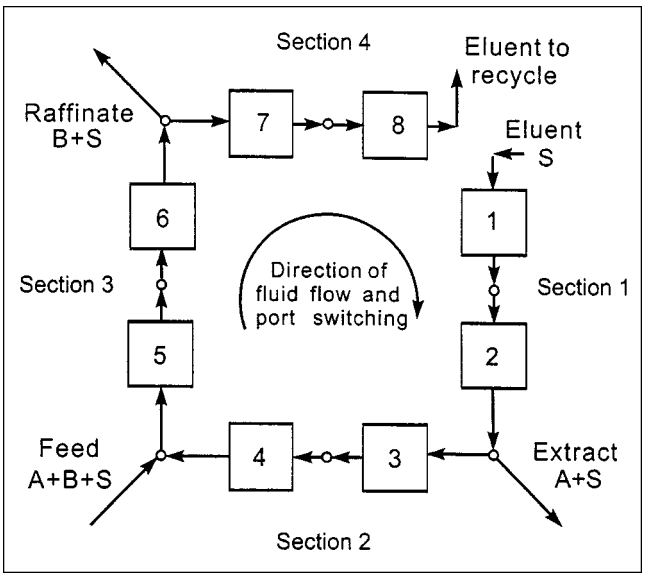

Figure 1. SMB pilot unit: 8 columns, 2-2-2-2 configuration.

The loop is open between section 4 and section 1.

The aim of this work is twofold. On the one hand, a shortcut design method for the design of nonlinear separations based on the Equilibrium Theory model is presented. This approach is different from solutions presented earlier that make use either of adsorption/desorption (Mallmann et al., 1999) or pulse experiments (Heuer et al., 1998). This solution aims at finding the approximate solution of the Equilibrium Theory model using both breakthrough and pulse experiments designed to minimize the amount of pure products needed. The experimental procedure is applied to a model system: the separation of the Tröger's base enantiomers on microcrystalline triacetate cellulose (CTA) (Pedeferri et al., 1999). This procedure is designed for the situation where, having already realized the SMB unit, one would like to use it for a new separation. This is a typical situation for multipurpose units in the types of industries mentioned earlier. On the other hand, we study the effect of the feed concentration on the separation performance of the SMB, which is of course the main source of nonlinearity in these systems. The experimental SMB results are discussed in light of the theoretical understanding of SMB behavior and the deviations from the ideal behavior due to mass-transfer resistance and extracolumn band broadening are assessed.

Experimental Setup

Columns and chemicals

Unsupported microcrystalline cellulose triacetate beads in the 15–25-μm size range (Merck 16362) were packed in a stainless-steel chromatographic column (0.46 cm ID $\times$ 25 cm). Some pulse experiments were carried out in a shorter column (0.46 cm ID $\times$ 5 cm). The stationary phase has been boiled in pure ethanol for 30 min to let it swell. The suspension was packed at room temperature under a pressure of 200 bar with ethanol as a pushing solvent at a flow rate of 4 cm^3/min. The pure (−)-TB and (+)-TB enantiomers have been purchased from Aldrich; all binary mixtures have been prepared by properly mixing the pure enantiomers. Pure ethanol used as the mobile phase as well as 1,3,5-tri-*ter*-butylbenzene (TTBB) used to measure the column porosity, have been purchased from Fluka and used as received. The purity of the Tröger's base used in the experiments is 99%.

Analytical methods

The analysis is performed under isocratic conditions on an HP 1100 liquid cromatograph equipped with a quaternary pump, an autosampler, and a thermostatted column compartment kept at 65°C. The flow rate is kept constant at a value of 0.5 cm^3/min. The chromatograph is connected in series with a UV detector (Jasco UV-970, wavelength 283 nm) and a polarimeter (Jasco OR-990). The data are collected through a computer data-acquisition system (sampling rate 0.25 s) and elaborated using a Labview program (Zenoni et al., 2000).

SMB pilot plant

The SMB unit has the open-loop 2-2-2-2 configuration, shown in Figure 1 (Pedeferri et al., 1999). The columns are located in a thermostatted chamber that is kept at a temperature of 65°C using a proper control scheme. Four flows (desorbent, extract, feed, and raffinate) are controlled by four HPLC pumps (Jasco PU-987). An on-line measurement of the weight of the feed and the product vessels (Mettler-Toledo 8700) allows us to cross-check the flow rates. The flows among the columns in the unit are managed by five (12 + 1)-port multiposition valves (Vici-Valco EMT-6-CSD12UW) connected to each of the eight columns. The distribution of extracolumn dead volumes is uneven, namely: $V_1^D = 1.21$ cm^3, $V_2^D = 2.30$ cm^3, $V_3^D = 1.21$ cm^3, $V_4^D = 1.76$ cm^3, (Pedeferri et al., 1999). During SMB runs, steady-state conditions have been considered to be attained when mass balances were fulfilled within a 3% maximum error.

Design of Operating Conditions

Before presenting the experimental shortcut design procedure, let us briefly summarize the criteria for the design of SMB separations under ideal conditions, that is, neglecting axial dispersion and mass-transfer resistance (Mazzotti et al., 1997). In this framework, that is, Equilibrium Theory, the separation performance depends on the generalized flow-rate ratios $\overline{m}_j$ in the four sections of the unit (Pedeferri et al., 1999; Migliorini et al., 1999b)

$$\overline{m}_j = \frac{Q_j t^* - V\epsilon^* - V_j^D}{V(1-\epsilon^*)}, \tag{1}$$

where all symbols are defined in the Notation section. This definition accounts for the effect of extracolumn dead volume and depends on the geometric properties of the SMB (column volume V, extracolumn dead volume V_j^D, and overall void fraction ϵ^*), the switch time t^*, and the flow rate Q_j in every section of the unit. The solution of the Equilibrium Theory model allows us to calculate the region of complete separation in the ($\overline{m}_2$, $\overline{m}_3$) plane (see Figure 2 and the con-

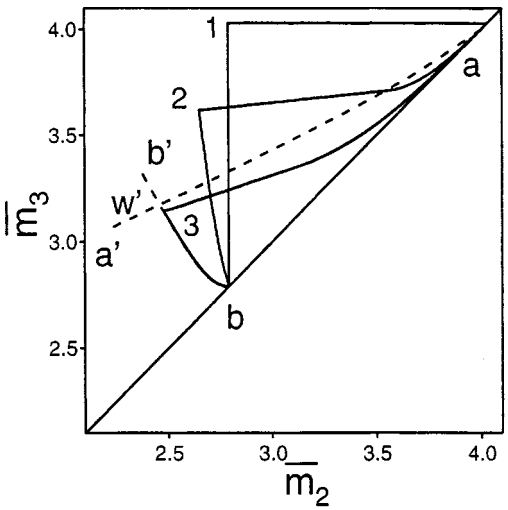

Figure 2. Effect of the feed concentration on the complete separation regions in the ($\overline{m}_2$, $\overline{m}_3$) plane for a bi-Langmuir isotherm (Migliorini et al., 2000a).

Infinite dilution $c_T^F \to 0$ (region 1); $c_T^F = 1.4$ g/L (region 2); and $c_T^F = 5.8$ g/L (region 3). The shortcut separation region bounded by ***bb'*** and ***aa'*** approximates the region of complete separation calculated rigorously by the Equilibrium Theory.

straints on the regenerating sections when the multicomponent equilibria are described with a linear (Ruthven and Ching, 1989), stoichiometric (Storti et al., 1993; Mazzotti et al., 1994; Chiang, 1998a,b), and non stoichiometric Langmuir (Mazzotti et al., 1996), bi-Langmuir (Gentilini et al., 1998), or IAS model (Migliorini et al., 2000a). If regeneration of the stationary and fluid phases is achieved in sections 1 and 4, complete separation is attained for the operating points belonging to the triangle-shaped region in the ($\overline{m}_2$, $\overline{m}_3$) plane in Figure 2 (Migliorini et al., 2000a).

Under linear conditions the amount adsorbed is proportional to the fluid-phase concentration, that is, $q_i = H_i c_i$. The following constraints must be fulfilled

$$\text{section 1:} \quad H_A \le \overline{m}_1 < \infty \tag{2}$$

$$\text{section 2:} \quad H_B \le \overline{m}_2 \le H_A \tag{3}$$

$$\text{section 3:} \quad H_B \le \overline{m}_3 \le H_A \tag{4}$$

$$\text{section 4:} \quad \frac{\epsilon_p}{\epsilon_p - 1} \le \overline{m}_4 \le H_B, \tag{5}$$

whose projection on the ($\overline{m}_2$,$\overline{m}_3$) plane defines the triangular separation region in Figure 1 (region 1). The coordinates of points ***a*** and ***b*** along the diagonal are given by the Henry constants of the more and less retained enantiomer, that is, H_A and H_B (here and in the following A denotes the more retained component). The Henry constants are usually determined from the retention times of a small racemic pulse, t_i^R

$$H_i = \frac{\left(t_i^R - t_0\right)}{t_0} \frac{\epsilon^*}{1 - \epsilon^*}, \tag{6}$$

where t_0 is the residence time of an inert tracer and the overall void fraction is given by

$$\epsilon^* = \frac{t_0 Q}{V}. \tag{7}$$

Shortcut approach

Under nonlinear conditions the shape of the separation region depends on the feed concentration and on the multicomponent adsorption equilibria. Accordingly, different isotherm models lead to separation regions of different shapes, even though under dilute condition they all converge to the same linear adsorption isotherm (Gentilini et al., 1998). As an example, the region of complete separation for a bi-Langmuir isotherm is shown in Figure 2. As the overall feed concentration, $c_T^F = c_A^F + c_B^F$, approaches zero, that is, when $c_T^F \to 0$, the bi-Langmuir model converges to the linear model and therefore the region of separation is the square triangle (region 1) defined by Eqs 3. to 4. As the feed concentration increases the vertex of the triangle, which is the point where the highest productivity is achieved (Mazzotti et al., 1997), moves to smaller $\overline{m}_2$ and $\overline{m}_3$ values and gets closer to the diagonal (see regions 2 and 3 in Figure 2). Such a deformation of the complete separation region is the result of the nonlinear competitive adsorption equilibria (Mazzotti et al., 1997).

The objective of this section is to estimate through a simple experimental procedure the region bounded by the curve ***bw'*** and the curve ***aw'***, which approximates the complete separation region obtained as a rigorous theoretical solution of the Equilibrium Theory model (Migliorini et al., 2000a). Here ***w'*** is the point of intersection of the curves ***bb'*** and ***aa'*** and represents an approximation of the optimal point of the complete separation region.

In the following we assume that the system exhibits a competitive adsorption behavior and that the transitions occurring during column adsorption and desorption experiments, are shocks and waves, respectively. These are rather general assumptions that apply to a large number of systems of interest [cf. Migliorini et al. (2000a) for a thorough discussion about this point]. In order to reduce the amount of experimental information needed, the curves ***bb'*** and ***aa'*** (see Figure 2) are approximated with straight lines, and therefore only one point along these lines is calculated (***a'*** and ***b'***), the other two points along the diagonal being the Henry constants (***a*** and ***b***).

The approximate region of complete separation corresponding to a mixture of feed composition (c_A^F, c_B^F) is then bounded by the following two straight lines:

• Straight line ***aa'***. The coordinates of point ***a'*** are given by

$$\overline{m}_2 = \frac{q_B\left(c_A^F, c_B^F\right)}{c_B^F} \tag{8}$$

$$\overline{m}_3 = \frac{q_A\left(c_A^F, c_B^F\right)}{c_A^F}, \tag{9}$$

which require the knowledge of the amount of A and B adsorbed at equilibrium with the liquid at the feed concentra-

tion (c_A^F, c_B^F). This can be readily estimated through a binary frontal experiment with the feed mixture during which the outlet concentration profiles of the two species are monitored, for example, using the on-line system described elsewhere (Zenoni et al., 2000).

• Straight line $\boldsymbol{bb'}$. The coordinates of point $\boldsymbol{b'}$ are given by

$$\overline{m}_2 = \left.\frac{\partial q_B}{\partial c_B}\right|_{(c_A^*,0)} = \left(\frac{t_B^* Q}{V} - \epsilon^*\right)\frac{1}{1-\epsilon^*} \tag{10}$$

$$\overline{m}_3 = \overline{m}_2 + \frac{q_A(c_A^*, 0) - \overline{m}_2 c_A^*}{c_A^F}. \tag{11}$$

Two pieces of information are needed in the last two equations. In Eq. 11 the adsorbed amount at equilibrium q_A (c_A^*,0) is measured through a frontal adsorption/desorption experiment with pure A; the best choice of the concentration level c_A^* is discussed in the next section. In Eq. 10 the quantity t_B^* indicates the retention time of the faster peak of the two obtained by injecting a pulse of the less retained enantiomer B on the plateau of composition (c_A^*, 0). The relationship (Eq. 10) between the retention time t_B^* and the derivative

$$\left.\frac{\partial q_B}{\partial c_B}\right|_{(c_A^*,0)}$$

has been proved previously (Zhong and Meunier, 1993; Tondeur et al., 1996); it holds true under the reasonable assumption that

$$\left.\frac{\partial q_B}{\partial c_A}\right|_{(c_A^*,0)}.$$

Experimental procedure

The procedure just presented is now applied to the separation of Tröger's base enantiomers on CTA under nonlinear conditions. This is particularly challenging because the separation is difficult due to the low efficiency of the stationary phase (Rizzi, 1989a,b). In addition, the more retained enantiomer exhibits unfavorable behavior at low concentrations (Seidel-Morgenstern and Guiochon, 1993; Pedeferri et al., 1999), thus leading to significant deviation from linear adsorption equilibria. However, the adsorption behavior is favorable at high concentrations, and the general assumption about the nature of the transitions (shocks and waves) is acceptable. The experimental procedure can be divided into the three following steps, which are summarized in Table 1.

Step 1: Pulse Experiments. A knowledge of the Henry constants allows us to calculate the complete separation region under linear conditions using Eqs. 3 and 4. These are estimated through racemic pulses of decreasing volume from 5 μL to 1 μL at a total concentration of 0.2 g/L. It has been verified that for the different injected volumes, the retention times obtained are the same, thus proving that the system operates under linear conditions. The Henry constants and the void fraction used are the average values obtained over the eight columns of the SMB unit, the maximum difference between pairs of values being 5% of the average value. These pulses on the clean columns yield $H_A = 3.5$ and $H_B = 1.9$, whereas tracer (TTBB) pulses yield $\epsilon^* = 0.56$ (Migliorini et al., 2000b). A knowledge of the Henry constants is also important for designing the regenerating sections. Let us consider the critical values for the flow-rate ratios in sections 1 and 4, that is, the lower bound $m_{1,cr}$ for m_1 and the upper bound $m_{4,cr}$ for m_4; under nonlinear conditions $m_{1,cr} = H_A$, but $m_{4,cr}$ is smaller than H_B, with a value depending on the feed concentration (Mazzotti et al., 1997; Migliorini et al., 1998a). In the experimental runs, a proper safety factor must be chosen to achieve complete regeneration, as discussed in the next section. A practical approach to determine $m_{4,cr}$, without the knowledge of the whole isotherm of the less retained species, can be to start the SMB separation experiments using the smallest m_4 value achievable and then increasing it until the performance of the separation gets worse. It is worth noting that the only disadvantage of having m_4 too small is more dilution in the raffinate stream, but this does not affect the product purity.

Step 2: Frontal Experiment and Hodograph Plane Analysis. The adsorbed equilibrium amounts q_A and q_B in Eqs. 8 and 9 are estimated by eluting the feed through a column initially saturated with the pure solvent. An on-line monitoring scheme that measures the concentration of the two enantiomers at the column outlet (see Figure 3) is used to calculate the area under each adsorption/desorption curve: each experiment allows us to repeat the measurement twice, thus providing a double check of the amount of each individual enantiomer adsorbed (Migliorini et al., 2000b). The following equilibrium loadings are estimated from these experiments: $q_A = 7.2$ g/L and $q_B = 3.4$ g/L at $c_T^F = 5$ g/L, and $q_A = 14.1$ g/L and $q_B = 8.8$ g/L at $c_T^F = 16$ g/L.

The results of the two runs are better analyzed in the hodograph plane shown in Figure 4, that is, the plane spanned by the concentrations of the two enantiomers. The transitions in the adsorption/desorption experiments are represented by the lines in the hodograph plane bearing the same label. The first transition, which is the breakthrough of the less retained species, is represented by a segment along the c_B axis labeled Σ_1. This transition is truncated at a point that is the intermediate state of the less retained species. The second transition

Table 1. Experimental Procedure to Determine the Approximate Complete Separation Region

Step 1.	Pulse experiments:	Henry constants
Step 2.	Binary frontal experiment:	amount adsorbed under competitive conditions at the feed concentration c_A^F, c_B^F
	Hodograph plane analysis:	analysis of the frontal runs to determine c_A^*
Step 3.	Single-component frontal experiment:	amount of pure enantiomers A adsorbed at the mobile-phase concentration c_A^*
	Pulse experiment:	retention time of the less ratained enantiomer t_B^* on a plateau of A at c_A^*

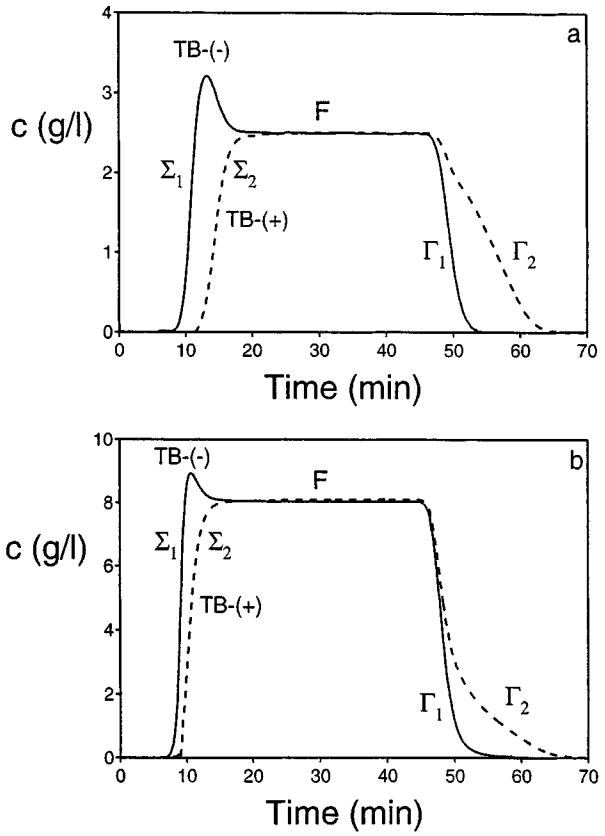

Figure 3. The experimental profiles for the adsorption/desorption step at the feed concentration of (a) $c_T^F = 5$ g/L, and (b) $c_T^F = 16$ g/L.

The relative composition is 50/50.

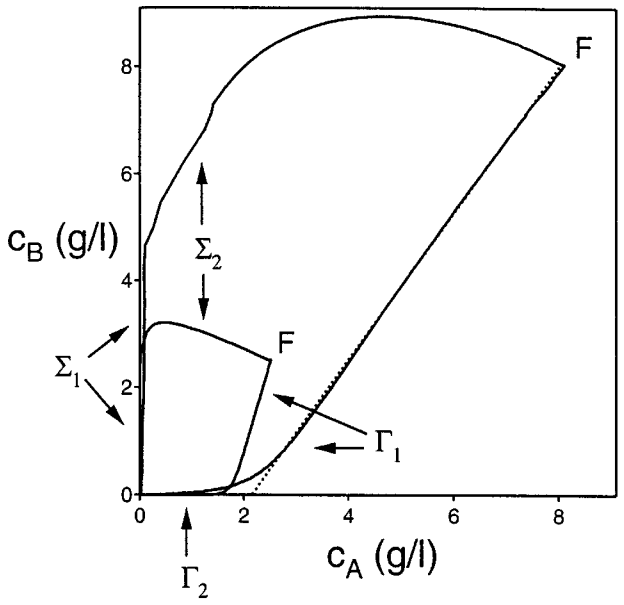

Figure 4. The adsorption/desorption experiments of Figure 3 in the hodograph plane.

The labels refer to the transition in Figure 3. The adsorption step is 40 min long. Solid line: experimental data; dotted line: linear extrapolation of Σ_1 to the axis c_A.

Σ_2 connects the intermediate state of B to the feed point F. In the desorption experiment, the first transition Γ_1 connects the feed point F to the intermediate state of the more retained component, which is finally eluted through the last transition Γ_2. It is worth noting that the hodograph plot for the adsorption/desorption experiments does *not* represent the transitions in the true counter current equivalent to the SMB unit, since in this case the intersection of Σ_1 and Γ_1 does not correspond to the feed composition [cf. Figure 6 in Migliorini et al. (2000a)].

Since the objective of this procedure is to approximate the region of separation close to the optimal conditions, in principle the pulse experiment should be run at a c_A^* value representative of the concentration of A achieved in section 2 under optimal conditions. This can be approximated as the concentration corresponding to the intersection of Γ_1 with the c_A axis, which actually provides a reliable upper estimate of the state attained in section 2 (Migliorini et al., 2000a).

In our example it is remarkable to notice that increasing the feed concentration does not change significantly the value of the intermediate state (see Figure 4). In the run at 5 g/L the intersection obtained by extrapolating linearly the transition Γ_1 to the axis is found to be $c_A = 1.7$ g/L, while in the run at 16 g/L, the intersection is about 2.1 g/L (dashed line in Figure 4). This behavior, that is, a small increase in the intermediate state for a large increase in the feed concentrations, is expected for binary competitive Langmuir systems when the concentration of the intermediate state approaches the watershed point (Rhee et al., 1989). In conclusion, the value $c_A^* = 2$ g/L is chosen as representative of the optimal conditions in section 2 for both runs.

The shape of the transitions in the hodograph plane for the two runs in Figure 3 is different. This is an effect of the low column efficiency, which is mainly responsible for bending the transitions Γ_1 and Σ_2 in the hodograph plane for the run at high concentration (Figure 3b). For instance, this can be seen in Figure 4, where Γ_1 exhibits a spread tail, and therefore the intermediate state is best approximated by a linear extrapolation of the transition at high concentrations. In addition, the transition Σ_2, which connects the peak of B due to the competitive adsorption of A with the feed plateau, is not monotonically decreasing like the run at low concentration. On the contrary, at high concentrations the concentration of B along Σ_2 appears first to increase, then to decrease when moving from the intermediate state to the feed state. This is surprising, since a higher competition, and therefore a higher peak, is expected at high concentrations. However, the low efficiency of the stationary phase and the small difference in the breakthrough time of the transitions Σ_1 and Σ_2 prevent the development of the full peak height.

Step 3: Frontal Analysis and Pulse Experiment. In order to estimate the derivative

$$\left.\frac{\partial q_B}{\partial c_B}\right|_{(c_A^*,0)}$$

in Eq. 10, pulse experiments with the less retained enantiomer and with $c_A^* = 2$ g/L are carried out. A 5-cm column is used in order to reduce the amount of the more retained

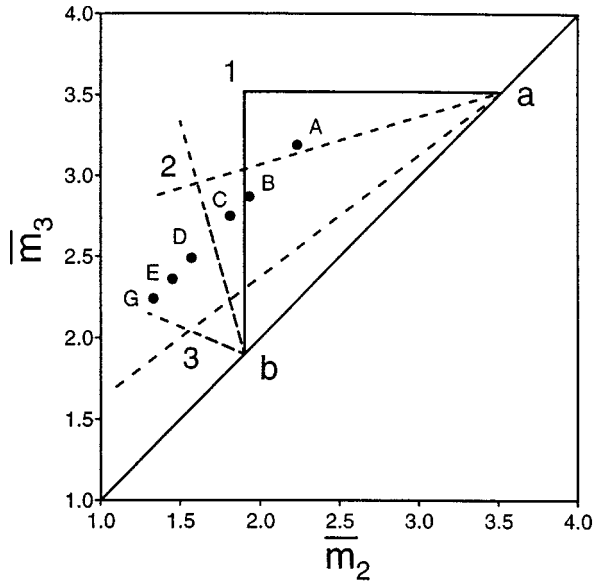

Figure 5. Separation of the Tröger's base racemic mixture.

Region of complete separation under linear conditions (region 1). Shortcut complete separation region at $c_T^F = 5$ g/L (region 2) and $c_T^F = 8$ g/L (region 3). Dots: experimental SMB runs.

enantiomer needed. After loading the column of the more retained enantiomer at 2 g/L, pulses at 50 and 30 μL of pure B at 0.15 g/L were carried out. Smaller volumes were not injected because the output signal becomes comparable to the intrinsic noise. These two pulses showed the same retention time, proving that the perturbation of the system is small enough to allow a proper estimation of the derivative in Eq. 10. The measured average retention time of the less retained enantiomer is $t_B^* = 130 \pm 3$ s. Finally, the column is desorbed, and the area under the adsorption and desorption outlet concentration yields the amount of pure A adsorbed at c_A^*, that is, $q(c_A^*,0)$. In this experiment the value $q_A(2, 0) = 6.11$ g/L is measured. From these experiments and Eqs. 10 and 11, it is possible to calculate the boundary ***bb'*** at the two concentrations of interest, as shown in Figure 5. It is worth noticing that the lines ***aa'*** and ***bb'*** at the two feed concentrations cross each other, as expected according to the theory. This behavior further confirms the reliability of this approach.

The approximations intrinsic to the proposed method do not have a dramatic impact on the results of Figure 5, since, for instance, the effect of axial dispersion and finite mass transfer should still be considered before analyzing the experimental performance. However, the shortcut method allows us to account quantitatively for the effect of the feed concentration, which leads to a smaller region of separation. In the next section these results are used to explain the performance of the SMB separation.

Effect of Feed Concentration on SMB Behavior

Many experimental results of SMB separations run under linear conditions have been reported in the literature (Yun et al., 1997a,b,c; Pedeferri et al., 1999). However, the effect of the feed concentration on the performance of the separation has not been investigated in detail yet [cf. Küsters et al. (1995) for two experimental runs of this type]. The first aim of this section is to fill this gap and to validate experimentally the behavior expected theoretically. The second aim is to show that the shortcut method is effective to design and interpret nonlinear SMB separations. The analysis of this section is carried out using the complete separation regions calculated in Figure 5. These regions are only an approximation of the real regions of separation, which could be calculated based on the complete knowledge of the adsorption equilibria. In addition, the experimental SMB results are affected by the low efficiency exhibited by the stationary phase and by the extracolumn dead volumes.

Table 2. Experimental Results for Separating Tröger's Base Enantiomers Using an 8-Column (2-2-2-2) SMB Unit

Run	t^* (min)	$\overline{m}_1$	$\overline{m}_2$	$\overline{m}_3$	$\overline{m}_4$	c_T^F(g/L)	P_E(%)	P_R(%)
A	42.5	8.26	2.23	3.20	−1.00	0.2	99.3	97.4
						5.0	98.5	93.9
B	40.0	7.64	1.93	2.87	−1.09	0.2	98.4	98.2
						5.0	98.1	95.1
C	39.0	7.39	1.81	2.75	−1.13	0.2	97.9	98.3
						5.0	97.4	98.6
						16.0	96.5	64.9
D	37.0	6.90	1.57	2.49	−1.20	0.2	94.5	98.6
						5.0	94.9	98.8
						16.0	96.7	75.6
E	36.0	6.65	1.45	2.36	−1.24	16.0	95.7	95.0
G	35.0	6.41	1.33	2.24	−1.27	16.0	95.2	98.1

Note:: The flow rates are $Q_1 = 0.410$ cm^3/min; $Q_2 = 0.200$ cm^3/min; $Q_3 = 0.212$ cm^3/min; $Q_4 = 0.061$ cm^3/min.

Six series of runs have been performed by keeping the flow rates constant and changing the switch time. The feed concentration has the values 0.2, 5, and 16 g/L of racemic mixture, as summarized in Table 2. The operating points belong to a straight line almost parallel to the diagonal, as shown in Figure 5. In this figure the regions of separation calculated at infinite dilution, at 5 and at 16 g/L using the shortcut approach, are also drawn. Notice that since the feed flow rate is constant in all the runs, the productivity of the plant is simply proportional to the feed concentration.

The purities of the raffinate stream are controlled by the position of the operating point in the ($\overline{m}_2$, $\overline{m}_3$) plane, provided that the regeneration of the solid phase in section 1 is effective. On the other hand, since the loop is open and the flow from section 4 is not recycled directly to section 1, the performance of section 4 in regenerating the mobile phase cannot affect the purity of the extract. Nevertheless in all our experiments the stream collected at the outlet of section 4 is always pure solvent, thus showing that the small $\overline{m}_4$ adopted guarantees regeneration of the mobile phase. To also prove that complete solid regeneration is attained in section 1, one can see that point G achieves a high raffinate purity ($> 98\%$) using the smallest $\overline{m}_1$ value (Table 1). This value is 1.8 times larger than the Henry constant of the more retained enantiomer, which is the lower bound for $\overline{m}_1$. In the other runs, a higher $\overline{m}_1$ value is always used, and therefore complete solid regeneration is always expected. Based on these considerations, it can be concluded that in all the runs discussed here

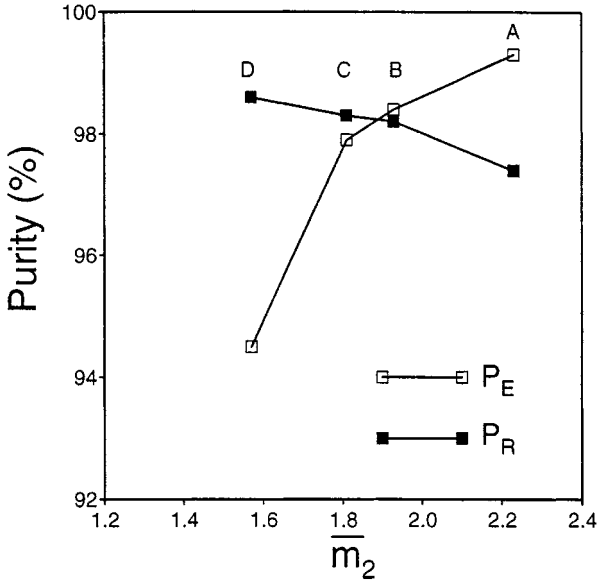

Figure 6. Purity of the extract and raffinate streams as a function of the operating parameter $\overline{m}_2$.

Feed concentration: 0.2 g/L racemic mixture.

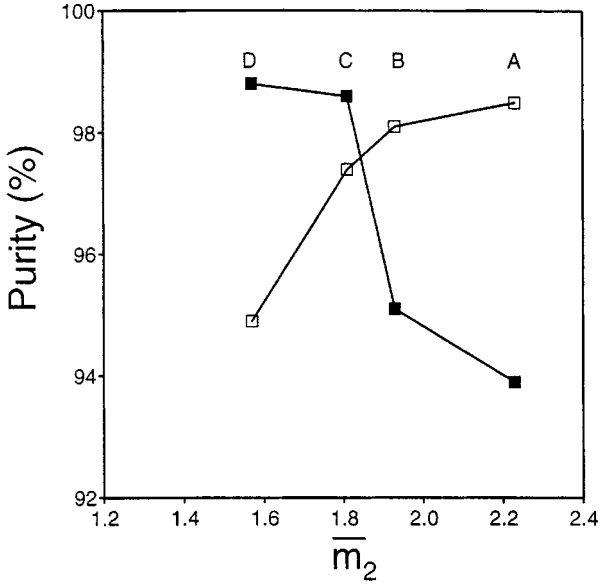

Figure 7. Purity of the extract and raffinate streams as a function of the operating parameter $\overline{m}_2$.

Feed concentration: 5.0 g/L racemic mixture.

the product purities depend only on the position of the operating point in the $(\overline{m}_2, \overline{m}_3)$ plane.

First, let us consider the runs at 0.2 g/L of feed concentration. As shown in Figure 6, in the series of experiments A to D the extract purities decrease from 99.3 % to 94.5%, while the raffinate purities increase from 97.4% to 98.6%. The operating point moves from the pure-extract region to the pure raffinate region, achieving the best symmetric purity performance in point B, where both purities are higher than 98%. Note that according to the previous work on the Tröger's base separation (Pedeferri et al., 1999), a point is thought to belong to the separation region when both purities are above 98%. Therefore point B in Figure 5 gives an indication of the position of the complete separation region at very low feed concentration. However, SMB separations on CTA can achieve higher purities. In these experiments the purities reached are limited by the purity of the feed mixture (which is $>99\%$) and the position of the operating points, which cannot be chosen closer to the diagonal due to the uneven distribution of the dead volumes in sections 2 and 3. In fact, when the dead volumes are unevenly distributed between sections 2 and 3 and $V_D^2 > V_D^3$, the region of separation in the $(\overline{m}_2, \overline{m}_3)$ plane below the line parallel to the diagonal and corresponding to the vanishing feed flow rate given by

$$\overline{m}_3 = \overline{m}_2 + \frac{V_D^2 - V_D^3}{V(1-\epsilon^*)}, \tag{12}$$

cannot be accessed. In other words, the extracolumn dead volumes not only shift but also shrink the separation region.

Concerning point A, it can be observed that a very high purity (99.3%) is obtained only in the extract, whereas the raffinate achieves only 97.4%. Even though this point lies in the calculated ideal complete-separation region in Figure 5, it could lie outside the actual region of separation. First of all, it must be considered that mass transfer shrinks the ideal region of separation. This effect is expected to be particularly strong under linear conditions where the self-sharpening tendency of the fronts due to nonlinear equilibria is not present (Migliorini et al., 1998b; Azevedo and Rodrigues, 1999). In addition, the region of separation (region 1 in Figure 5) is calculated under infinite dilution, while the experiment is run at a feed concentration of 0.2 g/L. The increase in the feed concentration moves the vertex downwards to the left, as shown in Figure 5. As a consequence, point A could be closer to the upper boundary than what Figure 5 shows, and therefore closer to the region where only the extract is pure. This explanation suggests that point B, which is close to the lower boundary of the ideal separation region, lies inside the actual complete separation region, as shown by the results in Figure 6.

Runs A, B, C, and D have been repeated at a feed concentration of 5 g/L, and the results are illustrated in Figure 7. Figures 6 and 7 exhibit a similar pattern of behavior of the extract and raffinate purities. However, two differences must be emphasized. First of all, an increase in productivity leads to a worse purity performance. In fact, in the runs at 5 g/L of feed concentration, the region of complete separation, that is, where both purities are higher than 98%, is never crossed, although the rather good performance in run C indicates that this point lies close to the optimal point of the complete separation region. The second difference is that the slope of the purity profiles in Figure 7 is sharper. In fact, under nonlinear conditions the region of separation becomes smaller in the neighborhood of the optimal point, as shown in Figure 2, and the operating conditions are less robust. The corresponding region of complete separation (region 2) in Figure 5 shows that A and D lie in the regions of pure extract and raffinate, according to the experimental results of Figure 7. In particular, the sharp decrease in the raffinate purity of A is the

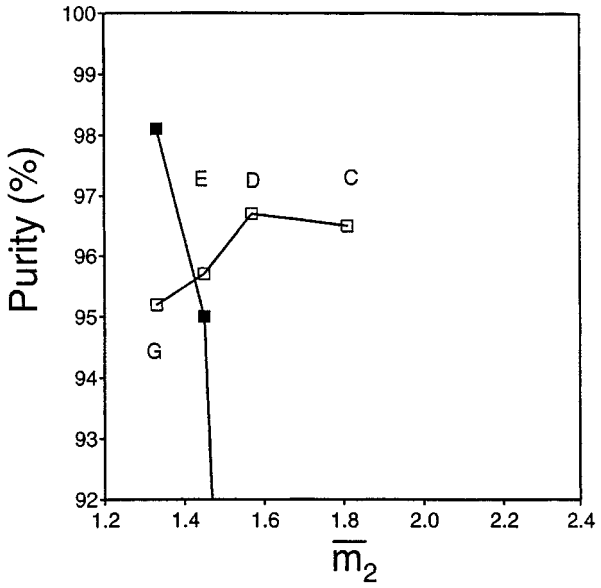

Figure 8. Purity of the extract and raffinate streams as a function of the operating parameter $\overline{m}_2$.

Feed concentration: 16 g/L racemic mixture.

effect of the shift in the boundary ***bb′*** of the separation region due to the increase in feed concentration. Although points *B* and *C* lie inside the separation region, purities lower than 98% are attained in the raffinate and the extract, respectively. This might again be due to mass-transfer limitations, which drive point *B* into the pure extract region and point *C* into the pure raffinate region.

The behavior for the runs at the feed concentration of 16 g/L is illustrated in Figure 8. As in Figure 7, these results show that higher feed concentrations lead to poorer performance. In fact, points *C*, *D* and *E* belong to the region where none of the two product streams is pure, while point *G* is in the pure raffinate region. A comparison between Figures 7 and 8 indicates that the point achieving symmetric purities shifts toward lower $\overline{m}_2$ values. This behavior parallels the shift of the optimal point shown in Figure 5. In fact, a symmetric purity in the extract and raffinate also is achieved in the region where there is no pure outlet above the optimal operating point. At a feed concentration of 16 g/L, higher purities could be achieved only by choosing operating points closer to the diagonal, for instance, by decreasing the feed flow rate.

Conclusions

This article presents a shortcut technique for designing SMB separations under nonlinear conditions. This allows us to approximate the region of separation based on the Equilibrium Theory model using a few experiments requiring only a small amount of pure products. First of all, pulses under dilute conditions allow the Henry constants to be calculated; these are then used to design the separation under linear conditions, as well as operating conditions for the regenerating sections. The information needed to draw the approximate regions of complete separation under nonlinear conditions are provided by adsorption/desorption runs at the concentration of the feed mixture and pulse experiments on a column loaded only with the more retained enantiomer.

The procedure is applied to the study of the resolution of the Tröger's base enantiomers on CTA; this is a rather difficult separation due to the low column efficiency. The experimental SMB runs at increasing feed concentration show how the nonlinear adsorption behavior affects the shape and the positions of the region of complete separation by shifting its optimal point toward lower $\overline{m}_2$ and $\overline{m}_3$ values in the ($\overline{m}_2$, $\overline{m}_3$) plane. The experiments also show that the separation performance of a small-scale SMB unit are very sensitive to the operating conditions. Changes in the switch time of one minute or less can lead to significant changes in the product purity. Therefore, the rational interpretation of the experimental results provided by this analysis is useful in reducing the number of experiments needed to optimize the operating conditions, particularly for a new separation without the detailed and lengthy measurement of the competitive adsorption isotherms.

Notation

c_i = fluid-phase concentration of species i
$\overline{m}_j$ = generalized flow-rate ratio in section j
q_i = adsorbed phase concentration of species i
Q_j = volumetric fluid flow rate in section j
t_0 = residence time of an inert tracer
t_i^R = retention time of species i
t^* = switch time
V = volume of a single adsorption column
V_j^D = extracolumn dead volume in section j

Greek letters

Γ = simple wave transition in the hodographic plane
ϵ^* = overall void fraction of the bed, defined as $\epsilon^* = \epsilon_b + (1-\epsilon_b)\epsilon_p$
ϵ_b = bed void fraction
ϵ_p = intraparticle void fraction
Σ = shock-wave transition in the hodographic plane

Subscripts and superscripts

A = more retained species
B = less retained species
cr = critical value
D = extracolumn dead volume
E = extract
F = feed
i = component index, $i = A,B$
j = section index, $j = 1, \ldots, 4$
R = raffinate
T = overall concentration

Literature Cited

Azevedo, D. C. S., and A. E. Rodrigues, "Design of SMB in the Presence of Mass Transfer Resistances," *AIChE J.*, **45**, 956 (1999).

Cavoy, E., M. F. Deltent, S. Lehoucq, and D. Miggiano, "Laboratory − Developed Simulated Moving Bed for Chiral Drug Separations. Design of the System and Separation of Tramadol Enantiomers," *J. Chromatog. A*, **769**, 49 (1997).

Charton, F., and R. M. Nicoud, "Complete Design of a Simulated Moving Bed," *J. Chromatog. A*, **702**, 97 (1995).

Chiang, A. S. T., "Complete Separation Conditions for a Local Equilibrium TCC Adsorption Unit," *AIChE J.*, **44**, 332 (1998a).

Chiang, A. S. T., "Equilibrium Theory for Simulated Moving Bed Adsorption Processes," *AIChE J.*, **44**, 2431 (1998b).

Francotte, E., and J. Richert, "Application of Simulated Moving Bed Chromatography to the Separation of the Enantiomers of Chiral Drugs," *J. Chromatog. A*, **769**, 101 (1997).

Francotte, E., J. Richert, M. Mazzotti, and M. Morbidelli, "Simulated Moving Bed Chromatographic Resolution of Racemic Guaifenesin," *J. Chromatog. A*, **796**, 239 (1998).
Gentilini, A., C. Migliorini, M. Mazzotti, and M. Morbidelli, "Optimal Operation of Simulated Moving Bed Units for Non-Linear Chromatographic Separations: II. Bi-Langmuir Isotherms," *J. Chromatog. A*, **805**, 37 (1998).
Guest, D. W., "Evaluation of Simulated Moving Bed Chromatography for Pharamceutical Process Development," *J. Chromatog. A*, **760**, 159 (1997).
Heuer, C., E. Küsters, T. Plattner, and A. Seidel-Morgenstern, "Design of the Simulated Moving Bed Process Based on Adsorption Isotherms Measurements Using a Perturbation Method," *J. Chromatog. A*, **827**, 175 (1998).
Küsters, E., G. Gerber, and F. D. Antia, "Enantioseparation of a Chiral Epoxide by Simulated Moving Bed Chromatography Using Chiralcel-OD," *Chromatographia*, **40**, 387 (1995).
Mallmann, T., B. D. Burris, Z. Ma, and N.-H. L. Wang, "Standing Wave Design of Nonlinear SMB Systems for Fructose Purification," *AIChE J.*, **44**, 2628 (1999).
Mazzotti, M., G. Storti, and M. Morbidelli, "Robust Design of Binary Countercurrent Separation Processes 2. Multicomponent Systems," *AIChE J.*, **40**, 1825 (1994).
Mazzotti, M., G. Stori, and M. Morbidelli, "Robust Design of Binary Countercurrent Separation Processes 3. Nonstoichiometric Systems," *AIChE J.*, **42**, 2784 (1996).
Mazzotti, M., G. Storti, and M. Morbidelli, "Optimal Operation of Simulated Moving Bed Units for Nonlinear Chromatographic Separations," *J. Chromatog. A*, **769**, 3 (1997).
Migliorini, C., M. Mazzotti, and M. Morbidelli, "Continuous Chromatographic Separation Through Simulated Moving Beds Under Linear and Nonlinear Conditions," *J. Chromatog. A*, **827**, 161 (1998a).
Migliorini, C., M. Mazzotti, and M. Morbidelli, "Modeling Simulated Moving Bed Units for the Separation of Fine Chemicals," *Fundamentals of Adsorption*, Vol. 98, Elsevier, Amsterdam, p. 484 (1998b).
Migliorini, C., A. Gentilini, M. Mazzotti, and M. Morbidelli, "Design of Simulated Moving Bed Units Under Non-Ideal Conditions," *Ind. Eng. Chem. Res.*, **38**, 2400 (1999a).
Migliorini, C., M. Mazzotti, and M. Morbidelli, "Simulated Moving Bed Units with Extracolumn Dead Volume," *AIChE J.*, **45**, 1411 (1999b).
Migliorini, C., M. Mazzotti, and M. Morbidelli, "Robust Design of Countercurrent Separation Processes 5. Non Constant Selectivity," *AIChE J.*, **46**, 1384 (2000a).
Migliorini, C., M. Mazzotti, G. Zenoni, M. Pedeferri, and M. Morbidelli, "Modeling Chromatographic Chiral Separations Under Nonlinear Competitive Conditions," *AIChE J.*, **46**, 1530 (2000b).
Nagamatsu, S., K. Murazumi, and S. Makino, "Chiral Separation of a Pharmaceutical Intermediate by a Simulated Moving Bed Process," *J. Chromatog. A*, **832**, 55 (1999).
Negawa, M., and F. Shoji, "Optical Resolution by Simulated Moving Bed Adsorption Technology," *J. Chromatog A*, **590**, 113 (1992).
Pais, L. S., J. M. Loureiro, and A. E. Rodrigues, "Modeling, Simulation and Operation of a Simulated Moving Bed for Continuous Chromatographic Separation of 1-1′-bi-2-Naphtol Enantiomers," *J. Chromatog. A*, **769**, 25 (1997).
Pedeferri, M., G. Zenoni, M. Mazzotti, and M. Morbidelli, "Experimental Analysis of a Chiral Separation Through Simulated Moving Bed Chromatography," *Chem. Eng. Sci.*, **54**, 3735 (1999).
Pröll, T., and E. Küsters, "Optimization Strategy for Simulated Moving Bed Systems," *J. Chromatog. A*, **800**, 135 (1998).
Rhee, H.-K., R. Aris, and N. R. Amundson, *First Order Partial Differential Equations*, Vol. II, Prentice-Hall, Englewood Cliffs, NJ (1989).
Rizzi, A. M., "Band Broadening in High-Performance Liquid Chromatographic Separations of Enantiomers with Swollen Microcrystalline Cellulose Triacetate Packings: I. Influence of Capacity Factor, Analyte Structure, Flow Velocity and Column Loading," *J. Chromatog.*, **478**, 71 (1989a).
Rizzi, A. M., "Band Broadening in High-Performance Liquid Chromatographic Separations of Enantiomers with Swollen Microcrystalline Cellulose Triacetate Packings: II. Influence of Eluent Composition, Temperature and Pressure," *J. Chromatogr.*, **478**, 87 (1989b).
Ruthven, D. M., and C. B. Ching, "Counter Current and Simulated Counter Current Adsorption Separation Processes," *Chem. Eng. Sci.*, **44**, 1011 (1989).
Seidel-Morgenstern, A., and G. Guiochon, "Modeling of the Competitive Isotherms and the Chromatographic Separation of Two Enantiomers," *Chem. Eng. Sci.*, **48**, 2787 (1993).
Storti, G., M. Mazzotti, M. Morbidelli, and S. Carrá, "Robust Design of Binary Countercurrent Separation Processes," *AIChE J.*, **39**, 471 (1993).
Tondeur, D., H. Kabir, L. A. Luo, and J. Granger, "Multicomponent Adsorption Equilibria from Impulse Response Chromatography," *Chem. Eng. Sci.*, **51**, 3781 (1996).
Wu, D.-J., Y. Xie, Z. Ma, and N.-H. L. Wang, "Design of Simulated Moving Bed Chromatography for Amino Acid Separations," *Ind. Eng. Chem. Res.*, **37**, 4023 (1998).
Yun, T., Z. Bensetiti, G. Zhong, and G. Guiochon, "Effect of Column Efficiency on the Internal Profiles and the Performance of a Simulated Moving Bed Unit in the Case of a Linear Isotherm," *J. Chromatog. A*, **758**, 175 (1997a).
Yun, T., G. Zhong, and G. Guiochon, "Experimental Study of the Influence of the Flow Rates in SMB Chromatography," *AIChE J.*, **43**, 2970 (1997b).
Yun, T., G. Zhong, and G. Guiochon, "Simulated Moving Bed Under Linear Conditions: Experimental vs. Calculated Results," *AIChE J.*, **43**, 935 (1997c).
Zenoni, G., M. Pedeferri, M. Mazzotti, and M. Morbidelli, "On-Line Monitoring of Enantiomer Concentration in Chiral Simulated Moving Bed Chromatography," *J. Chromatog A*, **888**, 73 (2000).
Zhong, G. M., and F. Meunier, "Linear Pertubation Chromatography Theory: Moment Solution for Two-Component Nonequilibrium Adsorption," *Chem. Eng. Sci.*, **48**, 1309 (1993).

Manuscript received March 27, 2000, and revision received June 20, 2001.